WPS1-PR(18) 20406

J Cosfeld et al.

Effective charge state modelling for Wendelstein 7-X edge plasmas

Preprint of Paper to be submitted for publication in
Nuclear Fusion

This work has been carried out within the framework of the EUROfusion Consortium and has received funding from the Euratom research and training programme 2014-2018 under grant agreement No 633053. The views and opinions expressed herein do not necessarily reflect those of the European Commission.

Effective charge state modelling for Wendelstein 7-X edge plasmas

J. Cosfeld[1], M. Rack[1,2], D. Reiter[1], P. Drews[1], B. Blackwell[3], M. Jakubowski[4], H. Niemann[4], D. Zhang[4], Y. Feng[4], and the Wendelstein 7-X Team

[1]Forschungszentrum Jülich GmbH, Insitut für Energie- und Klimaforschung – Plasmaphysik, Partner of the Trilateral Euregio Cluster (TEC), 52425 Jülich, Germany

[2] JARA-HPC, Jülich Supercomputing Centre, Forschungszentrum Jülich GmbH, 52425 Jülich, Germany

[3]Australian National University, Acton ACT, 2601 Canberra, Australia

[4]Max-Plank-Insitut für Plasmaphysik, 17491 Greifswald / 85748 Garching, Germany

E-mail: `j.cosfeld@fz-juelich.de`

Abstract. The three-dimensional Monte Carlo transport code package EMC3-EIRENE has been widely applied as edge plasma analysis tool for more than a decade now, resulting in successful validation applications against various measured trends seen in stellerator plasma boundaries. Here we apply this code package for Wendelstein 7-X discharges in interpretive mode. We are able to clearly identify (and correct) an earlier experimental hardware probe misalignment, which had led to an otherwise unresolvable inconsistency between experimentally constrained EMC3-EIRENE simulations and mid-plane Langmuir probe measurements.

Today W7-X plasma discharges still lack diagnostics to directly measure some important edge plasma properties, such as the spatial distribution of the effective charge state. Here EMC3-EIRENE simulations are applied in an iterative process to reconstruct these computationally. Earlier assumptions on the effective charge state distribution for reported Langmuir probe measurement have to be revised. Re-processing of up- and down-stream Langmuir probe measurements with code interpreted spatial profiles of the effective charge state now lead to overall improved physical consistency.

PACS numbers: 52.55Hc, 52.55.Fi, 52.65.Pp, 52.65Ww, 52.40.Hf

Keywords: Wendelstein 7-X, plasma-wall interaction, numerical diagnostic, EMC3-EIRENE

Submitted to: *Nuclear Fusion*

1. Introduction

Wendelstein 7-X (W7-X) [1] represents one of the most modern magnetic confinement fusion experiments today. It is based on an optimised stellerator magnetic configuration. W7-X has a modular set of 50 non-planar and 10 planar coils, to shape the geometry of the magnetic field in a favourable way [2]. Plasma dynamics within the complex three-dimensional structure of a stellerator can only partially be accessed by the installed diagnostics.

For this purpose the three-dimensional plasma edge code, which is treating complex magnetic field configurations with a fluid Monte-Carlo approach (EMC3) [3] coupled to the kinetic particle transport code EIRENE [4], is utilised in this study. EMC3 solves a set of macroscopic reduced Braginskii conservation equations [5] for the particle, parallel momenta and energies balance, while EIRENE solves multi-species Boltzmann equations of particles with internal states and inelastic collision processes. Both modules of the code package rely on Monte Carlo transport algorithms. In order to make connection with common terminology in numerical analysis [6], we note that for EMC3-EIRENE, non-linear coupling between the various equations and plasma components is carried out either conservatively directly within in the identity preserving Lagrangian "particle"-frame (e.g. for electron and ion energy, or for positive and negative ion momentum), in other cases Lagrangian quantities are first projected onto an intermediate (Eulerian) grid, and then re-sampled. EIRENE provides particle, momentum and energy sources and sinks from the kinetically treated components. Classical electron and main ion transport assumption (without kinetic corrections so far) is applied for the parallel heat transport in EMC3, while the perpendicular transport is treated by an anomalous diffusion ansatz. The implementation of light impurities (impurity ions with small atomic number Z) consists of a particular "trace fluid model" which allows only a small electron density perturbation by each impurity species. A one-dimensional (radial) core impurity model is an option which can be applied at the interface between the core plasma and the scrape-off layer [7] to set the proper boundary conditions for the not-fully ionised components. For this work a zero net flux across the core boundary was assumed.

In the first operational campaign W7-X was operated in limiter configuration [8, 9]. Different Langmuir probe diagnostics are installed on the limiter surfaces [10] and on the probe head of a multi-purpose manipulator (MPM) [11–13]. However, interpretation if these Langmuir probe measurement require information on the impurity content in the plasma. Diagnostics for the effective charge state distribution Z_{eff} measurements for examples, were not available in the first operational campaign of W7-X. Z_{eff} (constant or as profile) is a commonly used quantity for characterizing the global impurity content in the plasma [14].

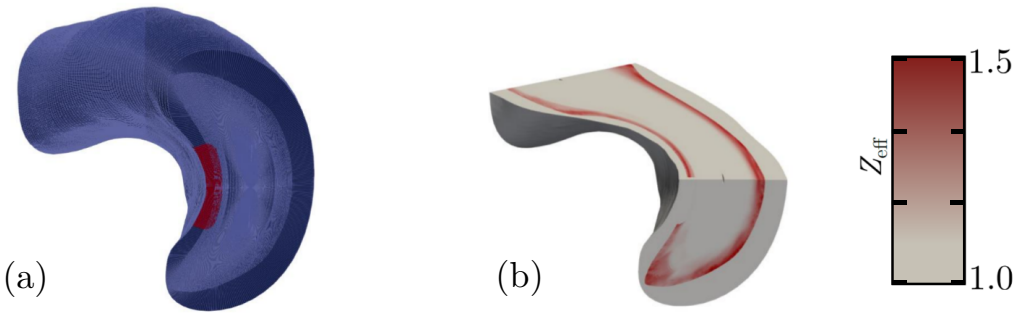

Figure 1: Overview of the computational domain of EMC3 (a) and an schematic two dimensional toroidal plot of Z_{eff}

Figure 1 gives a preliminary overview of the distribution of Z_{eff} in the experiment, accessed by EMC3-EIRENE.
It is shown in this publication that a remaining puzzle regarding the radial location of mid-plane Langmuir probes relative to the last close flux-surface (LCFS) was finally resolved by EMC3-EIRENE simulations. As a result of that, a consistency between plasma edge profiles (T_{e} and n_{e}) accessed by EMC3-EIRENE simulations and Langmuir probe measurements is achieved and discussed. To our knowledge no attempt has been made so far, to quantitatively reconstruct further plasma profiles, like Z_{eff}, from EMC3-EIRENE simulations which are consistent with several diagnostics and to include these plasma parameters in a refinement process of the Langmuir probe measurement interpretations. In the present paper a consistent reconstruction of Z_{eff}, via an iterative process between EMC3-EIRENE simulations and refined measurement datasets is achieved. This approach includes convergence criteria for deduce plasma parameters which lead to an final reconstruct charge state Z_{eff}. By the combination of the comparison- and reconstruction process, EMC3-EIRENE is applied as a three-dimensional interpretation tool for Wendelstein 7-X discharges.
The structure of this publication is as follows: First, in section 2, an overview of EMC3-EIRENE simulations used later in this paper will be given. Then, in section 3 the conditioning of EMC3-EIRENE simulations will be discussed. In particular, the beneficial impact of the EMC3-EIRENE simulations on Langmuir probe measurements, resulting in the assess of internal consistency between different Langmuir probe data sets, is investigated. In addition, the usage of EMC3-EIRENE as a complementary edge plasma diagnostic on W7-X will be discussed in section 4. The main results are summarized in the conclusion.

2. EMC3-EIRENE

In the EMC3-EIRENE Monte-Carlo code package, a 3D edge plasma transport model with a self-consistent iterative treatment of the plasma and neutral gas phases [4,15–17] is implemented. EMC3 solves a set of three-dimensional fluid equations in an externally

given magnetic field geometry. A detailed derivation of the EMC3 model equations can be found in [18]. Balance equations are solved for the quasineutral ($n_\mathrm{e} = n_\mathrm{i} = n$) plasma density n, the parallel momentum $u_\parallel$, and temperature T_α (with $\alpha \in \{\mathrm{e}, \mathrm{i}\}$) of single ion component plasma particles. They read, respectively:

$$\boldsymbol{\nabla} \cdot \left[n u_\parallel \hat{\mathbf{e}}_\parallel - D_\perp \boldsymbol{\nabla}_\perp n \right] = S_\mathrm{i} \quad , \tag{1}$$

$$\boldsymbol{\nabla} \cdot \left[m_\mathrm{i} n u_\parallel u_\parallel \hat{\mathbf{e}}_\parallel - \eta_\parallel \boldsymbol{\nabla}_\parallel u_\parallel - D_\perp \boldsymbol{\nabla}_\perp \left(m_\mathrm{i} n u_\parallel \right) \right] = -\hat{\mathbf{e}}_\parallel \cdot \boldsymbol{\nabla} p + S_\mathrm{m} \quad , \tag{2}$$

$$\boldsymbol{\nabla} \cdot \left[\frac{5}{2} n T_\alpha u_\parallel \hat{\mathbf{e}}_\parallel - \kappa_{\alpha\parallel} \boldsymbol{\nabla}_\parallel T_\alpha - \frac{5}{2} T_\alpha D_\perp \boldsymbol{\nabla}_\perp n - \chi_{\alpha\perp} n \boldsymbol{\nabla}_\perp T_\alpha \right] \tag{3}$$

$$= \xi \frac{3 m_\mathrm{i} n_\mathrm{e}}{m_\mathrm{e} \tau_\mathrm{ei}} \left(T_\mathrm{e} - T_\mathrm{i} \right) + S_{\mathrm{e},\alpha} - \delta_{\alpha\mathrm{e}} S_\mathrm{e,cool} \quad , \quad \xi = \begin{cases} +1 \ , \ \text{for } \alpha = \mathrm{i} \\ -1 \ , \ \text{for } \alpha = \mathrm{e} \end{cases}$$

where $\hat{\mathbf{e}}_\parallel$ is the unit vector in direction of the magnetic field and m_α represents the mass of the particle type α. The total plasma pressure p equals the sum of the electron plus ion temperature T_α times the density n: $p = n(T_\mathrm{e} + T_\mathrm{i})$. All EMC3 model equations are based on the plasma transport theory from Braginskii [5], with classical parallel transport coefficients $\eta_\parallel, \kappa_{\alpha,\parallel}$. The anomalous cross-field transport is taken into account by free model diffusion parameters $D_\perp$ and $\chi_{\mathrm{e,i}\perp}$.

The (aslo anomalous) perpendicular viscosity $\eta_\perp$ is re-expressed via combining the perpendicular components of the convective ($\boldsymbol{\nabla} \cdot [m_\mathrm{i} n V_{\mathrm{i}\parallel} \boldsymbol{V}_{\mathrm{i}\perp}]$]) and viscous stress $\boldsymbol{\nabla} \cdot [\eta_\perp \underline{\mathbf{I}}_\perp \cdot \boldsymbol{\nabla} V_{\mathrm{i}\parallel}]$ terms, using the perpendicular particle diffusion ansatz: $n \boldsymbol{V}_{\mathrm{i}\perp} = -D_\perp \boldsymbol{\nabla}_\perp n$. This yield the third term on the l.h.s. in (2), when furthermore the viscosity coefficient $\eta_\perp$ for viscous momentum fluxes due to perpendicular gradients in $V_\parallel$ is fixed by the ansatz $\eta_\perp = n m_\mathrm{i} D_\perp$ [17].

Interactions between neutrals and plasma electrons and ions are treated by the source terms S_i, S_m, and $S_{\mathrm{e},\alpha}$, which are obtained from the EIRENE code. Impurities released from plasma facing wall components cool the electrons via the energy sink $S_\mathrm{e,cool}$ appearing only in the electron energy balance. The attenuation effects on n_e due to impurity ions are still neglected, i.e. $n_\mathrm{e} = n_\mathrm{i}$, with the main ions i only. Only a strongly reduced parallel force balance model is used, rather than a full transport equation of the form of (2) supplemented by electric, frictional and thermal forces (which have been cancelled out between electrons and main plasma ions in (2)). A detailed discussion on the implementation of impurities into the edge modeling structure is given in the appendix. For this work, the five fold periodicity and the up-down stellerator symmetry [1] is taken into account. Therefore, the EMC3-EIRENE simulation grid in this work covers a toroidal segment of $\Delta\varphi_\mathrm{tor} = 36° = 36 \cdot \delta\varphi_\mathrm{tor}$ (with $\delta\varphi_\mathrm{tor}$ denoting the single toroidal element) with a resolution of $\Delta R = 3$ cm in radial direction, a poloidal grid of $\delta\theta_\mathrm{pol} = 1.5°$ for each of the 73 poloidal sections (with $\delta\theta_\mathrm{pol}$ denoting the single poloidal section). EMC3-EIRENE simulation are carried out on this grid to assess the

plasma edge dynamics with a full three-dimensional resolution.

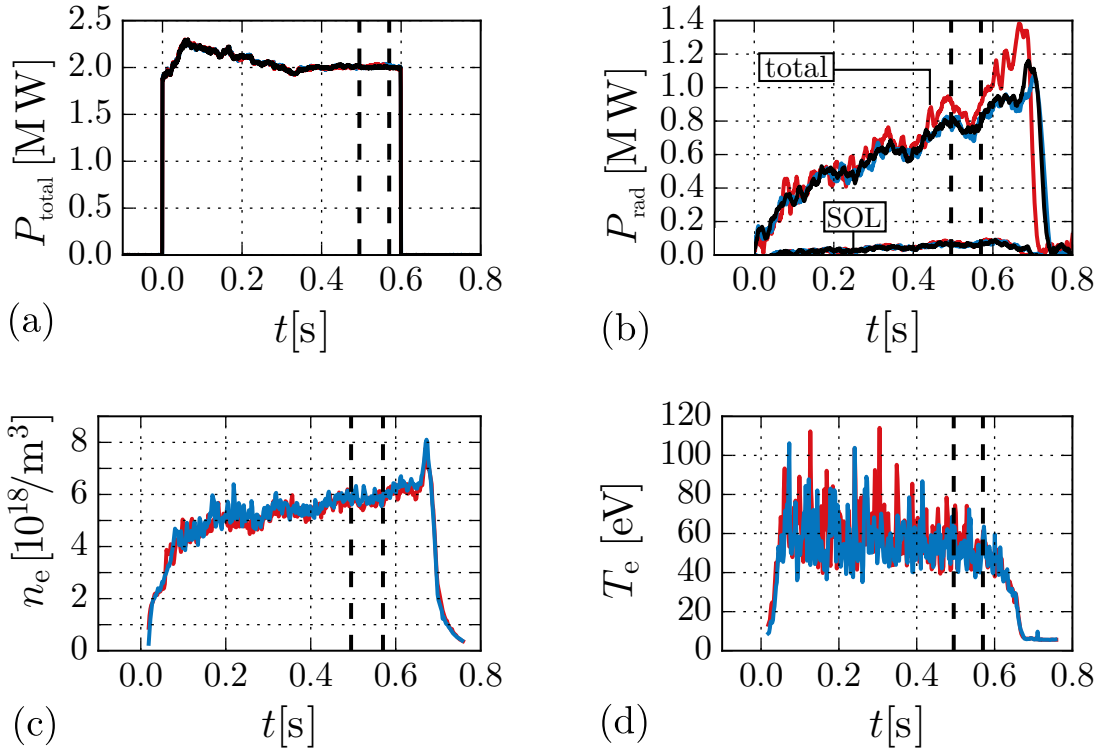

Figure 2: Overview of heating power (a), radiation (b) and down-stream n_{e} (c), T_{e} (d) measurements of a repetitive set of W7-X discharges. Color code refers to different discharges. Black: discharge 20160308.22, red: discharge 20160308.23 and blue: discharge 20160308.24. Up-stream Langmuir probe measurements were performed over a specific time interval Δt, indicated with the vertical dashed lines.

3. Experimentally constraining the EMC3-EIRENE simulations

In the following we consider EMC3-EIRENE simulations in combination with first down-stream Langmuir probe measurements [10]. The varied simulation parameters are transport coefficients $D_{\perp}$ and $\chi_{\text{e,i}}$, input heating power P_{heat}, radiated power P_{SOL} and the up-stream density n_{e}. They can be adjusted to match the measurements shown in figure 2. The chosen discharges were picked because of mid-plane n_{e} and T_{e} measurements which are only available for a small sub-set of all discharges. A manipulator plunged into the plasma over a time interval within the discharge duration $s = 0.05$ s (see figure dashed black lines 2). Resulting plasma parameters within the plunge time interval are taken to be input parameters for EMC3-EIRENE simulations. An overall heating power of 2 MW was applied of which in total 0.8 MW were radiated and thereby lost [19]. Considering all possible power losses, this adds up to an heating power entering the scrape-off layer (SOL) of $P_{\text{SOL}} = 1.32$ MW. By averaging the other measured plasma parameters over the specific time interval one obtains $P_{\text{rad}} = 120$ kW are radiated in the SOL, $n_{\text{e}} = 6 \times 10^{18}$ m^{-3} and $T_{\text{e}} = 50$ eV (measured down-stream)

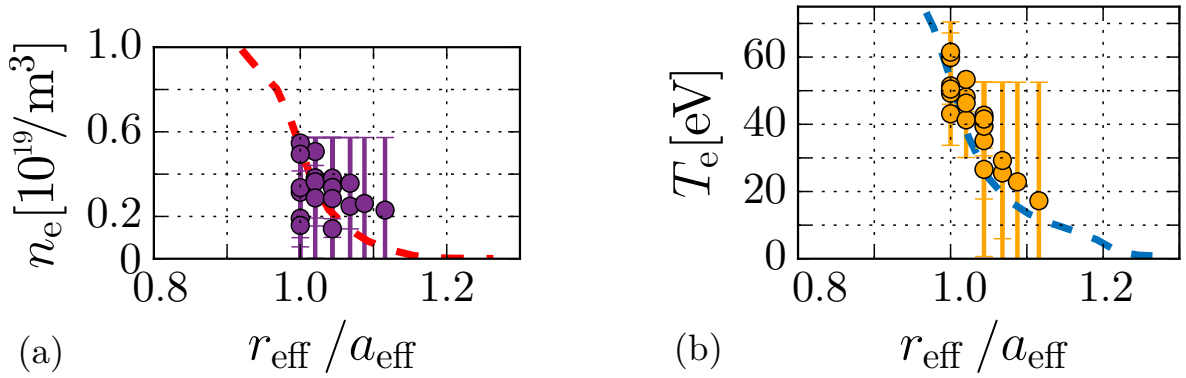

Figure 3: Comparison of density n_e (a) and temperature T_e (b) of EMC3-EIRENE simulation (dashed) and limiter Langmuir probe measurements (dots) plotted over the effective radius r_{eff}. Simulation parameters: $P_{SOL} = 1.32$ MW, $P_{rad} = 120$ kW, $n_e = 6 \times 10^{18}$ m^{-3} (down-stream), $T_e = 50$ eV (down-stream), $D_\perp = 0.5$ m^2/s and $\chi_{e,i} = 3D_\perp$.

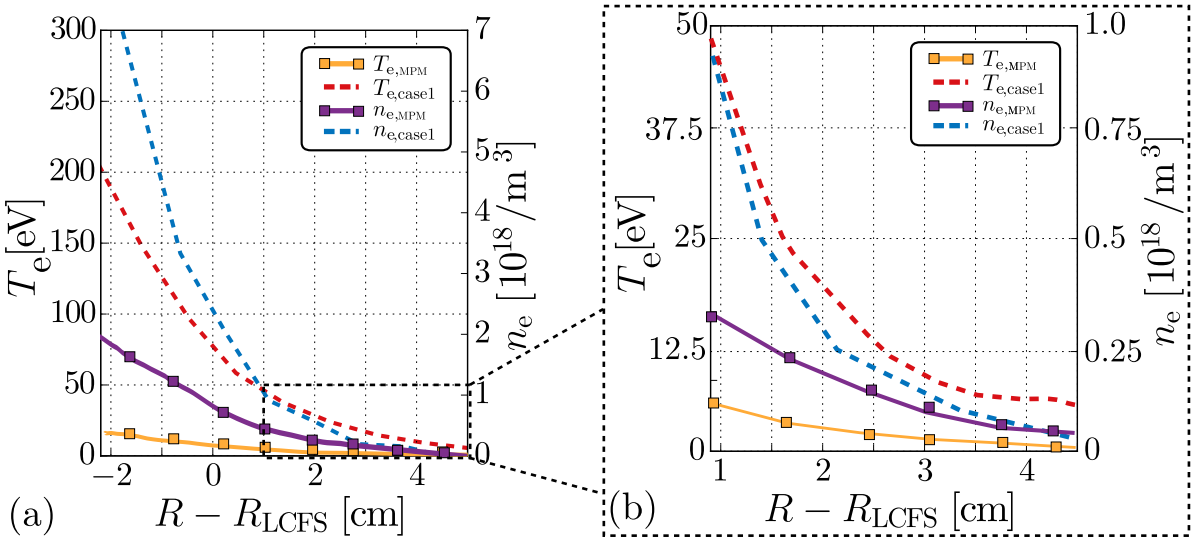

Figure 4: Comparison between EMC3-EIRENE simulation (dashed) and up-stream multi-purpose manipulator (MPM) measurements (solid) involving the uncorrected radial misalignment. Same simulation parameters as used in figure 3. Left hand plot (a) magnified in plot (b).

for the input parameters of EMC3-EIRENE. **Case1** will refer to this simulation setup from now on.

In addition to what is presented in figure 2, the limiter Langmuir probes are spatially resolved in radial direction. Therefore, a comparison between simulations and measurements allows a detailed discussion of radial profiles of n_e and T_e in comparison to up-stream measurements [11].

Consequently, a simulation with the input parameters of **case1** should also show a good agreement to up-stream measurements. However, this is clearly not true for **case1** as the left plot of figure 4 depicts. Nevertheless, plasma edge profiles of the simulation

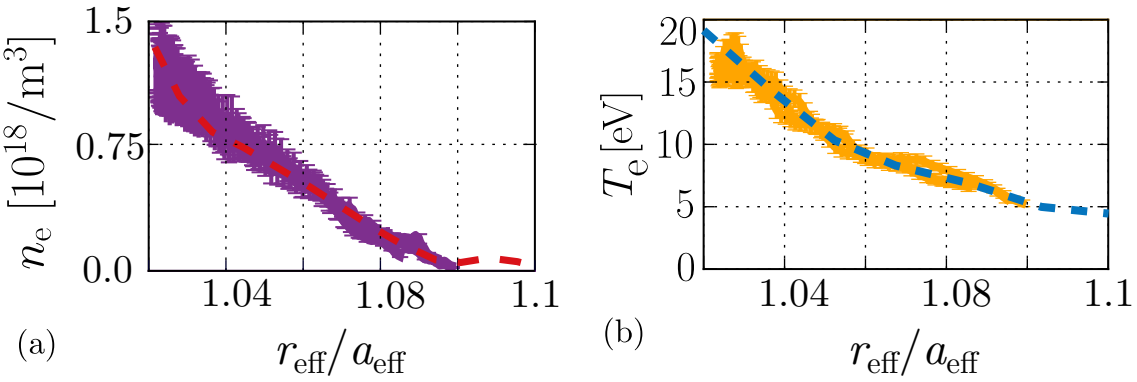

Figure 5: Comparison between EMC3-EIRENE simulation (dashed) and MPM measurements (solid with colored error bars) with corrected probe positioning at the up-stream measurement location. Same simulation parameters as used in figure 3.

lie in scope of the Langmuir probe measurements around 4 cm radially away from the last closed flux-surface (LCFS) $R - R_{\mathrm{LCFS}} = 4$ cm. This led us to consider a radial misalignment of the up-stream Langmuir probe measurement. A radial shift of 4 cm was found to be necessary to obtain good agreement between simulation and measurement (see figure 4).
This radial offset prediction was then indeed independently confirmed by a necessary experimental hardware re-adjustment. The offset was found to be roughly 6 cm. Finally, a comparison of the plasma edge profiles from EMC3-EIRENE to the experimental data sets including the corrected up-stream probe positioning resulted in a good overall agreement and consistency, on the down-stream measurement location (see figure 3) and on the up-stream (see figure 5) measurement location. Furthermore, the limiter heat flux measurements [20, 21] provide a third reference point for further constraining EMC3-EIRENE simulations. Here, radial heat flux profiles along the limiter at $Z = -0.2$ m are discussed.

Figure 6 shows heat-flux profiles onto the left section of one limiter plotted against the effective radius r_{eff}. The radial heat flux profiles of the measurement, are also consistent to EMC3-EIRENE simulation results of **case1**. Likewise, the up- and down-stream Langmuir probe measurements, simulation results of **case1** show a good agreement to the heat flux measurement.

4. 3D spatially resolved effective charge state reconstruction

In this section we discuss the effective charge state $Z_{\mathrm{eff}} = \sum n_Z Z^2 / \sum n_Z Z$ profiles and thus extract information for the processing of the measurement analysis of e.g. Langmuir probes. EMC3-EIRENE enables direct access to the densities of every single

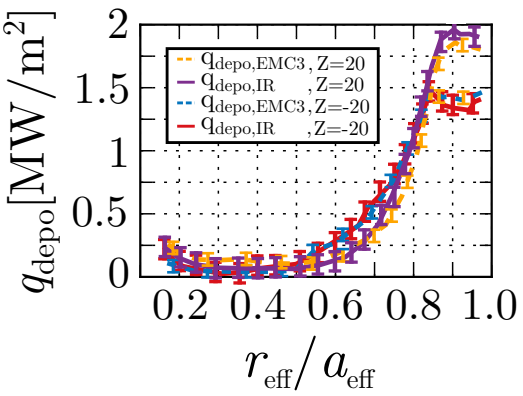

Figure 6: Comparison between EMC3-EIRENE simulation (dashed) and heat flux measurements (solid). Same simulation parameters as used in figure 3.

ionization state of the impurity ions (under the mentioned simplifying assumptions) and one can easily deduce the local charge state Z_{eff}. These profiles were not directly measurable during the limiter campaign [1,9]. Therefore, assumptions for Z_{eff} along the Langmuir probe location had to be made. $Z_{\mathrm{eff}} = 1$ was initially assumed at both, up- and down-stream, measurement locations (see figure 3 and 5), the plasma is assumed to be a pure hydrogen plasma. Hence, the calculation of the electron density from the saturation current I_{sat} (used in the data interpretation process in [11]), measured by the Langmuir probes, is affected by a change of Z_{eff} profiles.

$$n_{\mathrm{e,MPM}} = \frac{I_{\mathrm{sat}}}{0.49 A_{\mathrm{eff}} \sqrt{\frac{T_{\mathrm{i}}(r) + Z_{\mathrm{eff}}(r) T_{\mathrm{e}}(r)}{m_{\mathrm{i}}}}} \quad . \tag{4}$$

The simulation using the setup for **case1** clearly shows that these assumptions are not valid (see figure 7 (a)).
However, the first wall contains materials with a higher atomic number Z than hydrogen [1]. In measured discharges, as presented in figure 2, highly energetic particles reach the plasma facing wall components. These higher energy particles pollute the fusion plasma with impurities. Therefore, the overall effective charge state Z_{eff} of the plasma is changed. Hence, a recalibration of the measurements (see figure 8), using the presumably more plausible Z_{eff} profiles shown in figure 7 allows a correction of the measurements. Obviously, this needs to be followed by an adjustment of the simulation as one of the constrains change, visual by the offset between $n_{\mathrm{e,EMC3}}$ and $n_{\mathrm{e,MPM}}$ (see figure 8).
The discussed comparison process from section 3, to match measurements with EMC3-ERIENE simulations, needs to be reconsidered. For this purpose, an iterative process is used from this set of EMC3-EIRENE simulations, where each simulation refers to an iterative step i. Z_{eff} profiles will be deduced from the simulations in each iterative step i

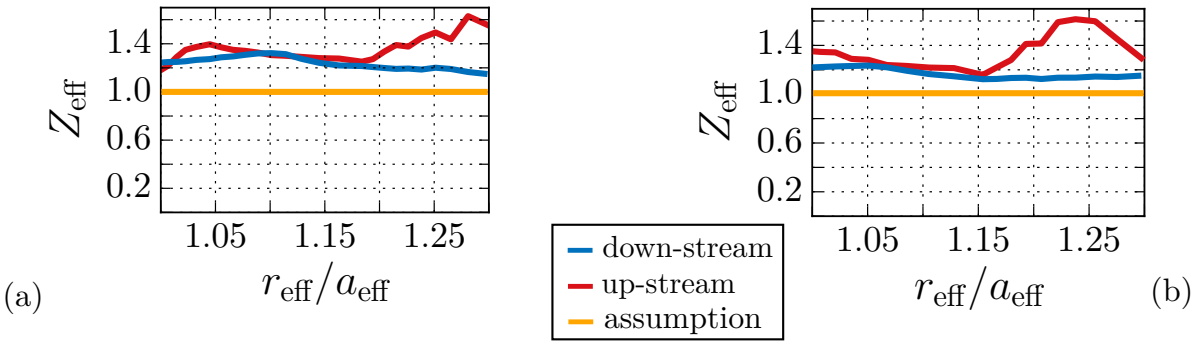

(a) (b)

Figure 7: Z_{eff} at up- and down-stream measurement location in comparison to made assumption for the measurement locations. Simulation **case1** (a), converged simulation **case2** (b)

and used in recalibration of the measurement. A schematic overview of the first iterative step is shown in figure 8, each sub-figure (reaching from (a) to (d)) is cosponsoring to the sub-steps of the first iterative step. The schematic overview discusses the iterative process for the up-stream multi purpose manipulator (MPM) measurements. It should be noted that the iterative process is also applied to down-stream Langmuir probe measurements. Density profiles measured by the MPM (up-stream) are used as reference in figure 8. The first iterative step begins with the access of Z_{eff} (sub-step (a) and (b), see figure 8) from the n_{e} profiles shown in figure 5. In the next sub-step (c) of figure 8, a updated $n_{\mathrm{e,MPM}}^{\mathrm{refined}}$ profile including the accessed $Z_{\mathrm{eff}}^{\mathrm{up-stream}}$ profiles is shown. Hence, one can note a displacement regarding $n_{\mathrm{e,MPM}}$ in a comparison of sub-step (a) and sub-step (c) shown in figure 8. This introduced displacement of $n_{\mathrm{e,MPM}}$ must be matched with the input parameters of EMC3-EIRENE. For sub-step (d), a switch from an input density (discussed in chapter 2) of $n_{\mathrm{e}} = 3 \times 10^{18}$ m^{-3} to 3.1×10^{18} m^{-3} was found to be suitable to match $n_{\mathrm{e,MPM}}$ of sub-step (c) with $n_{\mathrm{e,EMC3}}$. The fist iterative step is completed, since the consistency is between $n_{\mathrm{e,MPM}}^{\mathrm{refined}}$ and $n_{\mathrm{e,EMC3}}$ is again achieved. The relative deviation of the EMC3-EIRENE density profile $n_{\mathrm{e,EMC3}}$ and $n_{\mathrm{e,MPM}}$ is calculated via,

$$\delta_{\mathrm{relative,up}} = \mathrm{mean}\left(\frac{n_{\mathrm{e,EMC3}} - n_{\mathrm{e,MPM}}}{n_{\mathrm{e,EMC3}}}\right) \quad . \tag{5}$$

This measure is used to quantify the convergence of the density profiles to each other. The relative deviation $\delta_{\mathrm{relative,up}}$ is plotted for sub-step (c) and (d), a drop of $\delta_{\mathrm{relative,up}}$ is obverveable between sub-step (c) and (d). A additional conformation regarding the consitency between plasma edge modeling and MPM measurement. Subsequently, the next iteration steps are carried out following the same scheme of sub-steps as shown and discussed in figure 8. The appropriate factor ε^{i+1} for a recalibration of the input

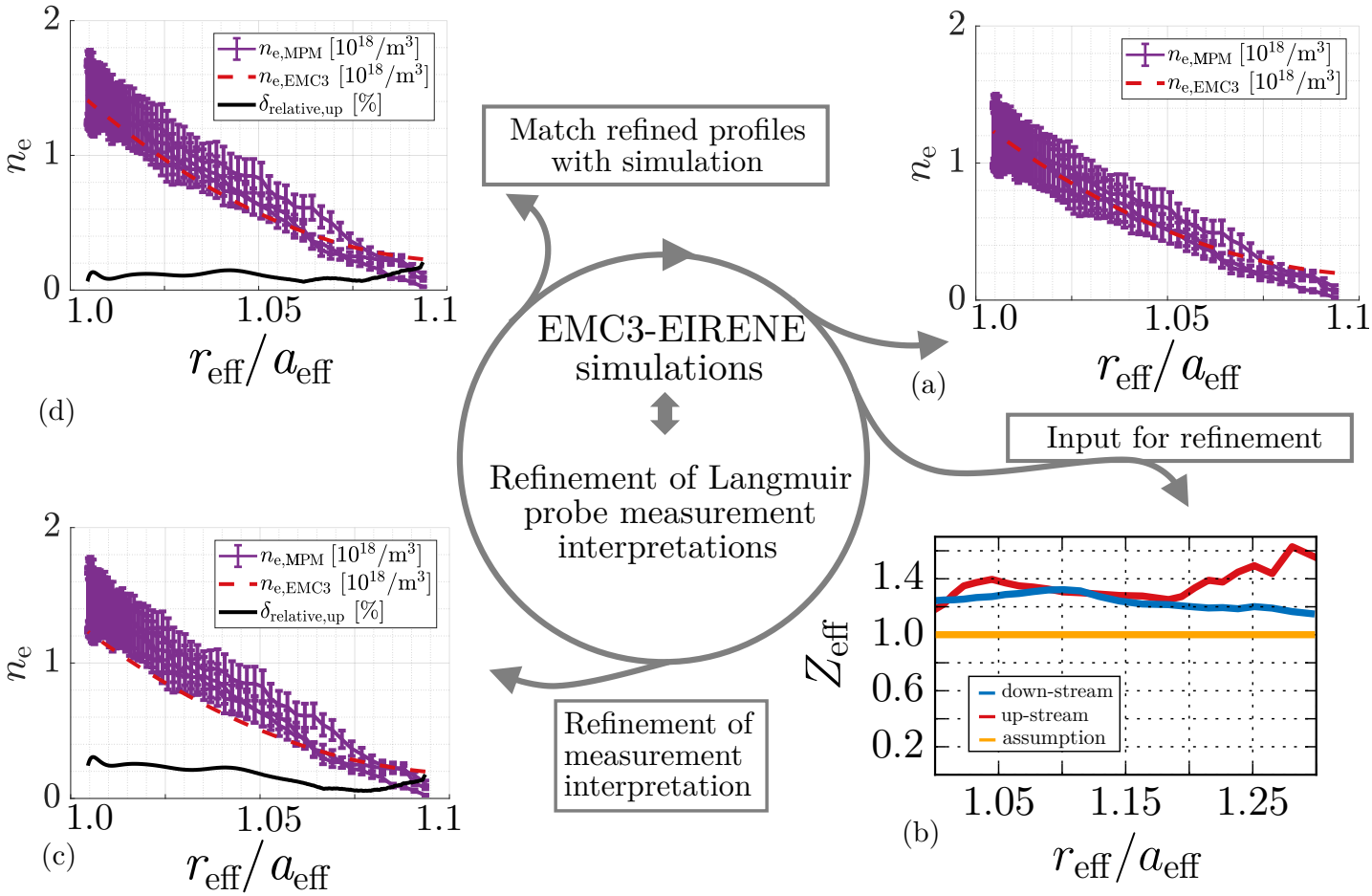

Figure 8: Schematic overview of the first iterative step of the iterative process. Electron density form **case1** shown in (a), Z_{eff} was assumed for $n_{\text{e,MPM}}$. Deduced Z_{eff} profiles shown in (b). Relative deviation $\delta_{\text{relative,up}}$ (see equation (5)) plotted into the comparison plot of the numeric and measured density data-set(c) and (d). The rework of plot 5 is shown in (d). Same simulation parameters as used in figure 3 in (a), input density was iterated to an up-stream density of 3.5×10^{18} m^{-3} in (b).

parameter n_e of the simulation for the iterative step $i+1$ can be quantified in:

$$\varepsilon^{i+1} = \frac{n_{\text{e,MPM}}(Z^i_{\text{eff}})}{n_{\text{e,MPM}}(Z^{i-1}_{\text{eff}})} = \sqrt{\frac{1+Z^i_{\text{eff}}}{1+Z^{i-1}_{\text{eff}}}} \quad . \tag{6}$$

Each Langmuir probe data-set was updated with the profile of the effective charge state Z^i_{eff} from the simulation to which the $n_{\text{e,MPM}}$ profile was compared one iterative step before. Hence, a $n_{\text{e,EMC3}}$ profile which is coinciding to the profile of the Langmuir probe measurement $n_{\text{e,MPM}}$ is also leading to a convergence of the Z^i_{eff} profile (see figure 8). **Case2** will refer to the simulation setup with the smallest relative deviation $\delta_{\text{relative,up}}$. Figure 9 shows on the left hand side the relative deviation calculated by equation 5. The relative deviation $\delta_{\text{relative,up}}$ drops below 1% for an numerical up-stream density of 3.5×10^{18} m^{-3}. **Case2** is referring to this particular simulation. As the input density

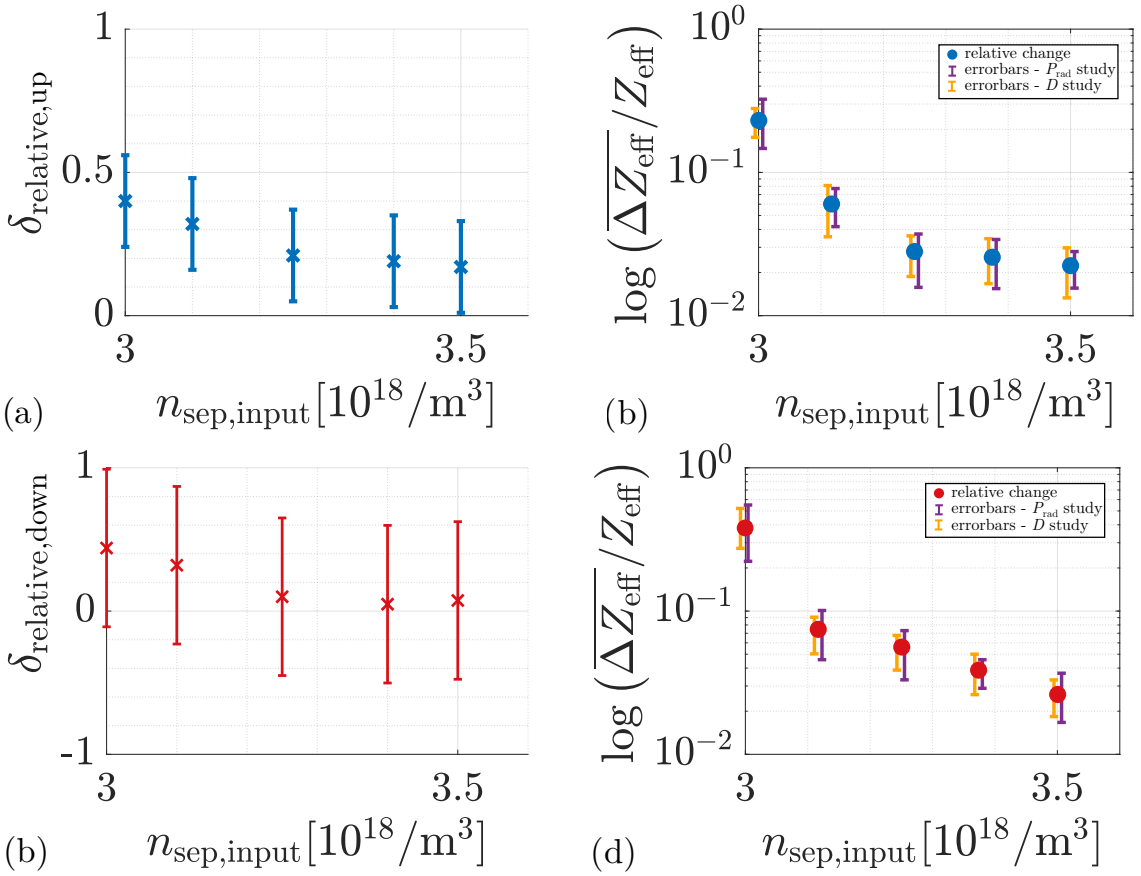

Figure 9: Relative deviation $\delta_{\text{relative,\{up,down\}}}$ plotted against the density of each iteration step (a) and (c). The change of the averaged Z_{eff} profile plotted against the density of each iteration step (b) and (d). Same simulation parameters as used in figure 3 (a) and (c), input density was iterated up to 3.5×10^{18} m^{-3}. Orange error bars are due to a influence study of the diffusion coefficient ($D \in [0.4,\ 0.5,\ 0.6]\ \frac{\text{m}^2}{s}$), magenta error bars due to a influence study of the lost power due to radiation ($P_{\text{rad}} = [60,\ 120,\ 180]$ kW)

is iterated from 3×10^{18} m^{-3} to 3.5×10^{18} m^{-3} the change of the Z_{eff} (calculated via $\log\left(\overline{\Delta Z_{\text{eff}}}/Z_{\text{eff}}\right)$) profile at the up-stream location is reduced to values below 1%. The relative change for the density values at the down-stream position $\delta_{\text{relative,up}}$ shows large error bars. This is due to the limiter Langmuir probe measurements which where performed with eroded probe heads, consequently density data sets have to be treated with caution. Figure 7 shows up- and down-stream Z_{eff} profiles of the last iterative step using the simulation setup **case2**. As the relative deviation $\delta_{\text{relative,up}}$ for the up-stream region is converged to a value below 1%, an overall good agreement between the measurement and simulation is shown as final result in figure 11 on the right hand side. Shown measured density profiles are refined by 12% to more correct and consistent profiles. In section 3 simulation **case1** provided an overall good agreement to the Langmuir probe measurements at the up- and down-stream location. Now, the simulation **case2** shows again an overall good agreement for both different

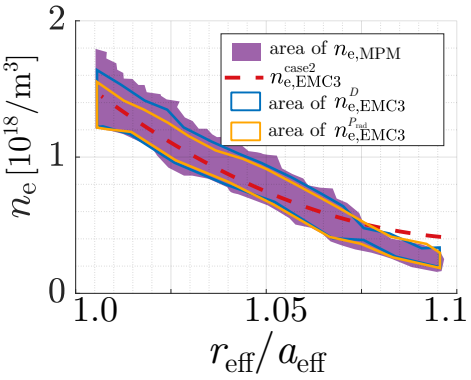

Figure 10: Overview of the of the influence of a variation over D and P_{rad} on $n_{\mathrm{e,EMC3}}$, plotted in translucent areas which entail the simulation results for $n^{\mathrm{D}}_{\mathrm{e,EMC3}}$ and $n^{\mathrm{P_{rad}}}_{\mathrm{e,EMC3}}$. Plotted in comparison to the magenta shaded area of $n_{\mathrm{e,MPM}}$ and the guide to the eye $n^{\mathrm{case2}}_{\mathrm{e,EMC3}}$

measurement locations including also, additionally a more reasonable estimate for up- and down-stream Z_{eff} profiles. Furthermore, the iterative process leads to a convergence of the estimated Z_{eff} profiles which directly affect Langmuir probe data processing. Additionally, each simulations setup shown in figure 11 was accompanied by a scan over the diffusion coefficient and the radiated Power P_{rad}. Free input parameters like D underlie an initial guess. A sensitivity study for $n_{\mathrm{e,ecm3}}$ concerning D and P_{rad} (free input parameters) is performed, to cover the influence of these free simulation parameters. D is chosen in $D \in [0.4,\ 0.5,\ 0.6]\ \frac{\mathrm{m}^2}{s}$ and P_{rad} is chosen in $P_{\mathrm{rad}} = [60,\ 120,\ 180]$ kW for each iterative step. The variation of D and P_{rad} resulted in both cases for each iterative step in profiles which again show a consistency between $n_{\mathrm{e,EMC3}}$ and $n_{\mathrm{e,MPM}}$.
The resulting change of $n_{\mathrm{e,EMC3}}$ is observable in the enclosed are of $n^{\mathrm{D}}_{\mathrm{e,EMC3}}$ and $n^{\mathrm{P_{rad}}}_{\mathrm{e,EMC3}}$ of figure 10. The overlap of the simulations results of the simulation results $n_{\mathrm{e,EMC3}}$ and measurement $n_{\mathrm{e,MPM}}$ (with error bars) remains high, thus the consistency between $n_{\mathrm{e,EMC3}}$ and $n_{\mathrm{e,MPM}}$ is preserved concerning the variation of D and P_{rad}.

5. Conclusions

The EMC3-EIRENE code has been applied to support diagnostic processing for three-dimensionally resolved edge plasma parameter measurements. The computational approach allowed a clear identification of a radial hardware offset of four centimeters regarding the positioning of the manipulator. Interpretative EMC3-EIRENE simulations are also used to assess plasma parameters which are currently not directly accessible by any diagnostic available on W7-X . Inferred spatial Z_{eff} profiles were identified as further sensitive input information for the data processing of several W7-X diagnostics, especially Langmuir probes, as these diagnostics rely on the knowledge of

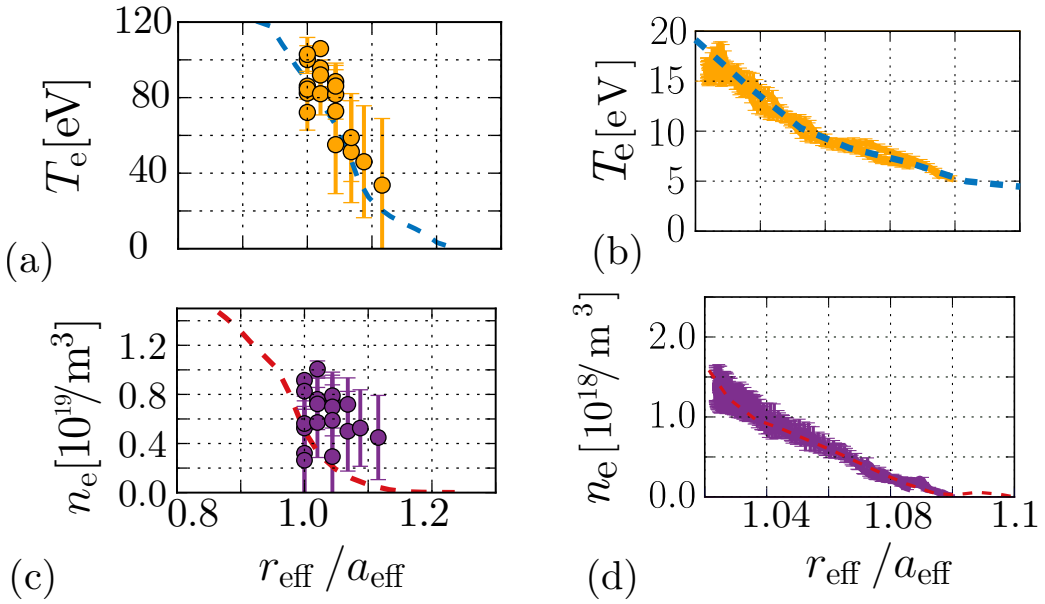

Figure 11: Final comparison between EMC3-EIRENE simulation (dashed) and Z_{eff} adjusted limiter Langmuir probes (a) and (c) - manipulator Langmuir probe (b) and (d) - measurements (solid). Same simulation parameters as used in figure 3 in (a) and (c), input density was iterated to be 3.5×10^{18} m^{-3}.

radial Z_{eff} profiles at their position. An iterative reprocessing of the Langmuir probe data was performed in comparison to EMC3-EIRENE simulations. This finally led to fully 3D resolved edge plasma simulation which lies in overall good agreement with the available up- and down-stream measurements, including Z_{eff} consistent with measured radiative power losses.

We conclude that more generally in particular in 3D magnetic configurations, edge plasma diagnostics, which rely on assumptions over spatial plasma parameter distributions such as Z_{eff} can profit from this complementary "numerical" diagnostic.

Further model refinements, in particular in the trace impurity ion fluid model, and comparison of simulations to further W7-X diagnostics are steps which have to be taken in the future, in particular when oxygen, with its (hitherto neglected) accidental charge exchange resonance, remains a relevant plasma impurity in W7-X discharges.

Acknowledgments

We are thankful for the valuable discussions with Dirk Reiser, Felix Reimold and Glen Wurden. The authors gratefully acknowledge the computing time granted by the JARA-HPC Vergabegremium and VSR commission on the supercomputer JURECA at Forschungszentrum Jülich. This work has been carried out within the framework of the EUROfusion Consortium and has received funding from the Euratom research

and training programme 2014-2018 under grant agreement no. 633053. The views and opinions expressed here in do not necessarily reflect those of the European Commission.

Appendix. Discussion of the impurity model.

The parallel impurity force balance (species/charge state α) in EMC3 reads ($\hat{\mathbf{e}}_\parallel \cdot \boldsymbol{\nabla} = \nabla_\parallel,\ p_\alpha = n_\alpha T_\alpha$)

$$0 = -\hat{\mathbf{e}}_\parallel \cdot \boldsymbol{\nabla} p + Z_\alpha n_\alpha e E_\parallel + \frac{\mu_{\alpha i}}{\tau_{\alpha i}} n_\alpha (u_{i\parallel} - u_{\alpha\parallel}) + \alpha_{\alpha e} n_\alpha \nabla_\parallel T_e + + \beta_{\alpha i} n_\alpha \nabla_\parallel T_i + S_{\mathrm{m}\alpha}\ . \quad (7)$$

with the pressure gradient force, electric force, frictional force, electron and ion thermal force, respectively. The momentum sources $S_{\mathrm{m}\alpha}$ due to ionisation, recombination with neighbouring charge states as well as due to interaction of impurity ion α with any of the kinetically treated species in EIRENE is neglected: $S_{\mathrm{m}\alpha} = 0$. μ is the reduced mass, and the collision times τ and electron-ion thermal force coefficients $\alpha_{\alpha e} = 0.71 Z_\alpha^2$ are again taken from Braginskii [5]. A low impurity concentration limit ($n_\alpha \ll n_i$) expression for the ion-ion thermal force coefficient $\beta_{\alpha i}$ is used, which was originally derived by S. Chapman (1958), and later frequently employed as approximation in tokamak and stellarator edge transport models [22]:

$$\beta_{\alpha i} = -3\ \frac{1 - \tilde{\mu} - 5\sqrt{2}(Z_\alpha/Z_i)^2\ (1.1\tilde{\mu}^{5/2} - 0.35\tilde{\mu}^{3/2})}{2.6 - 2\tilde{\mu} + 5.4\tilde{\mu}^2}, \quad \tilde{\mu} = \frac{m_\alpha}{m_\alpha + m_i}\quad . \quad (8)$$

As usual, instead of the Poisson equation the common "plasma approximation" is made to express the parallel electric field in (7) via the (here strongly reduced) electron momentum balance (neglecting all terms containing the electron mass):

$$e E_\parallel = -\frac{1}{n_e} \nabla_\parallel p_e - \alpha_{ie} \nabla_\parallel T_e \quad (9)$$

Inserting this into (7) provides the explicit expression for the parallel impurity ion flow velocity $u_{\alpha\parallel}$:

$$u_{\alpha\parallel} = u_{i\parallel} + \frac{\tau_{\alpha i}}{\mu_{\alpha i}} \left[(\beta_{\alpha i} - 1) \nabla_\parallel T_i - \frac{Z_\alpha}{n_e} \nabla_\parallel p_e + (\alpha_{\alpha e} - Z_\alpha \alpha_{ie}) \nabla_\parallel T_e \right] + \frac{\tau_{\alpha i}}{\mu_{\alpha i} n_\alpha} T_i \nabla_\parallel n_\alpha \quad . \quad (10)$$

Denoting the first part on the r.h.s. by $U_{\alpha\parallel}$ and introducing the (binary) diffusion coefficient due to friction between main ions and impurity ions $D^f_{\alpha\parallel} = \frac{\tau_{\alpha i} T_i}{\mu_{\alpha i}}$ a diffusion - advection expression for the parallel impurity ion flux Γ_α results:

$$\Gamma_{\alpha\parallel} = n_\alpha u_{\alpha\parallel} = n_\alpha U_{\alpha\parallel} - D^f_{\alpha\parallel} \nabla_\parallel n_\alpha \quad . \quad (11)$$

Inserting (11) into (1) leads to an impurity continuity equation:

$$\boldsymbol{\nabla} \cdot \left[n_\alpha U_{\alpha\parallel} \hat{\mathbf{e}}_\parallel - D^f_{\alpha\parallel} \nabla_\parallel n_\alpha - D_\perp \boldsymbol{\nabla}_\perp n_\alpha \right] = S_\alpha \quad . \quad (12)$$

In addition, $T_\alpha = T_\mathrm{i}$ is assumed for all impurity species α, and each charge state is treated as a separate fluid. The (particle) source term S_α provides the coupling between neighboring charge states due to ionisation and recombination, and, for the single charged impurity ion, the ionisation rate from neutral impurity atoms. The latter are launched, mono-energetically, from target surfaces with a given sputtering rate, and then simply exponentially decayed due to ionisation into the plasma. Again the identity preserving Lagrangian scheme mentioned above is utilised for the transfer from neutral to ionised impurities (rather than re-sampling from volumetric neutral impurity sources), distinct from the current re-sampling coupling procedure for neutrals and molecules treated fully kinetically by EIRENE. There is, in principle no limitation on the number of impurity species (within the trace impurity transport model), as long as the concentration of the impurities is limited by the assumption $n_\alpha \ll n_\mathrm{e}$ and inter-impurity effects other than those in the source terms can be neglected.
Equation (12) for n_α is then coupled to the electron energy balance equation (3) of the main plasma, via the cooling term $S_{e,cool}$. A detailed discussion of impurity radiation and the resulting cooling effect on the energy balance equation (3) is given in [17]. Within an iterative process a self-consistent solution for the mentioned plasma parameters, $n, T_\alpha, u_\parallel, n_\alpha$ and $S_\mathrm{e,cool}$ is obtained. Impurities return back into the edge region with the same charge as they entered the core region, i.e. the net flux across the core boundary is set to zero for each charge state individually. Furthermore: a toroidally and poloidally homogeneous density is enforced for each charge state, on that core boundary. A radial decay length of 4 cm for n and T_α is implemented as boundary condition for the outer radial first wall boundary throughout this work. Impurities which reach the target are absorbed.

References

[1] T. Klinger et al. Performance and properties of the first plasmas of Wendelstein 7-X. *Plasma Physics and Controlled Fusion*, 59(1):014018, 2017.

[2] C.D. Beidler et al. Physics and engineering design for Wendelstein 7-X. *Fusion Technology*, 17(1):148–168, 1990.

[3] Y. Feng. 3D fluid modelling of the edge plasma by means of a Monte Carlo technique. *Journal of Nuclear Materials*, 266-269:812–818, 1999.

[4] D. Reiter. The EIRENE and B2-EIRENE Codes. *Fusion Science and Technology*, 47:172–186, 2005.

[5] S. I. Braginskii. Transport Processes in a Plasma. *Reviews of Plasma Physics*, 1:205, 1965.

[6] Angela Diggs and S. Balachandar. Modeling and simulation challenges in eulerian-lagrangian computations of multiphase flows. *AIP Conference Proceedings*, 1793(1):150008, 2017.

[7] Y. Feng et al. Recent Improvements in the EMC3-Eirene Code. *Contributions to Plasma Physics*, 54(4-6):426–431, 2014.

[8] T. S. Pedersen et al. Plans for the first plasma operation of Wendelstein 7-X. *Nuclear Fusion*, 55(12):126001, 2015.

[9] R. Wolf et al. Major results from the first plasma campaign of the Wendelstein 7-X stellarator. 57, 06 2017.

[10] M. Krychowiak et al. Overview of diagnostic performance and results for the first operation phase in Wendelstein 7-X. *Review of Scientific Instruments*, 87(11):11D304, 2016.

[11] P. Drews et al. Measurement of the plasma edge profiles using the combined probe on W7-X. *Nuclear Fusion*, 57(12):126020, 2017.

[12] D. Nicolai et al. A multi-purpose manipulator system for W7-X as user facility for plasma edge investigation. *Fusion Engineering and Design*, 123(Supplement C):960 – 964, 2017. Proceedings of the 29th Symposium on Fusion Technology (SOFT-29) Prague, Czech Republic, September 5-9, 2016.

[13] G. Satheeswaran et al. A PCS7-based control and safety system for operation of the W7-X Multi-Purpose Manipulator facility. *Fusion Engineering and Design*, 123(Supplement C):699 – 702, 2017. Proceedings of the 29th Symposium on Fusion Technology (SOFT-29) Prague, Czech Republic, September 5-9, 2016.

[14] H. Meister et al. An integrated system to measure the effective charge of fusion plasmas in the ASDEX Upgrade tokamak. *Review of Scientific Instruments*, 74(11):4625–4633, 2003.

[15] Y. Feng et al. 3D edge modeling and island divertor physics. *Contributions to Plasma Physics*, 44 (1-3):57–69, 2004.

[16] D. Reiter. Randschicht-Konfiguration von Tokamaks. Entwicklung und Anwendung stochastischer Modelle zur Beschreibung des Neutralgastransports. 0366-0885(1947), 1984.

[17] M. Rack et al. A fluid-kinetic approach for 3D plasma edge transport in He plasma. *Nuclear Fusion*, 57 (5):056011, 2017.

[18] D. Harting et al. 3D Monte-Carlo-Simulationen der ergodisierten Randschicht von TEXTOR-DED. *Technical Report*, Jül(4173), 2005.

[19] M. Hirsch et al. Confinement in Wendelstein 7-X limiter plasmas. *Nuclear Fusion*, 57(8):086010, 2017.

[20] H. Niemann et al. Power loads in the limiter phase of Wendelstein 7-X. 4:5, 2016.

[21] F. Effenberg. Numerical investigation of plasma edge transport and limiter heat fluxes in Wendelstein 7-X startup plasmas with EMC3-EIRENE. *Nuclear Fusion*, 57, 2017.

[22] J. Neuhauser. Modelling of impurity flow in the tokamak scrape-off layer. *Nuclear Fusion*, 24:39, 1984.